remote sensing

MDPI

Article

IR Thermography from UAVs to Monitor Thermal Anomalies in the Envelopes of Traditional Wine Cellars: Field Test

Juan Ortiz-Sanz [1], Mariluz Gil-Docampo [1], Marcos Arza-García [1,*] and Ignacio Cañas-Guerrero [2]

[1] Agroforestry Engineering Department, University of Santiago de Compostela (USC), Higher Polytechnic School of Engineering, 27002 Lugo, Spain; j.ortiz@usc.es (J.O.-S.); ml.gil@usc.es (M.G.-D.)

[2] Agroforestry Engineering Department, Polytechnic University of Madrid (UPM), School of Agricultural, Food and Biosystems Engineering, 28040 Madrid, Spain; ignacio.canas@upm.es

* Correspondence: m.arza@usc.es

Received: 7 May 2019; Accepted: 13 June 2019; Published: 14 June 2019

Abstract: Infrared thermography (IRT) techniques for building inspection are currently becoming increasingly popular as non-destructive methods that provide valuable information about surface temperature (ST) and ST contrast (delta-T). With the advent of unmanned aerial vehicle (UAV)-mounted thermal cameras, IRT technology is now endowed with improved flexibility from an aerial perspective for the study of building envelopes. A case study cellar in Northwest (NW) Spain is used to assess the capability and reliability of low-altitude passive IRT in evaluating a typical semi-buried building. The study comparatively assesses the use of a pole-mounted FLIR B335 camera and a drone-mounted FLIR Vue Pro R camera for this purpose. Both tested IRT systems demonstrate good effectiveness in detecting thermal anomalies (e.g., thermal bridges, air leakages, constructive singularities, and moisture in the walls of the cellar) but pose some difficulties in performing accurate ST measurements under real operating conditions. Working with UAVs gives great flexibility for the inspection, but the angle of view strongly influences the radiometric data captured and must be taken into account to avoid disturbances due to specular reflections.

Keywords: drone; thermal inspection; heat leaks; cellar; winery; thermal bridges; infrared thermography; wine maturation; UAS

1. Introduction

Temperature influences almost every step of wine production, starting with the growing of the grape [1], but is particularly important for several reactions involved in the process of wine maturation [2,3]. Since many of these reactions are physiochemical in nature, they can be accelerated with high temperatures [4,5]. Overall, ignoring the singularities of each wine variety, to reduce wine losses and prevent rapid ageing and loss of quality, the wines should be stored at a cool cellar ambient air temperature (AAT). The final wine quality can be more precisely controlled by using the method of AAT monitoring inside the ageing rooms [6] or even sensors embedded inside wine barrels [7].

The introduction of modern cooling systems to the wine industry has allowed excellent wines to be produced almost anywhere in the world, with a high degree of independence from the surrounding climate. However, energy use during wine production still represents a high percentage of the total electricity used by the winery [8]. Many studies highlight some advantages of traditional cellars over modern construction practices from the viewpoint of energy savings [9,10]. The bioclimatic strategies of these buildings encompass suitable management of thermal inertia (frequently through the use of buried or semi-buried structures, which benefit from the high thermal inertia of the ground) [11], in

most cases together with an adequate orientation and appropriate natural ventilation [12]. The new global strategies and energy directives towards achieving nearly zero-energy buildings have again put value on many of these traditional buildings for winemaking.

Nevertheless, materials might not perform as expected, and it is quite common to find mismatches between predicted and actual performance in buildings [13–17]. For this reason, thermal bridges, essential components of the transmission heat loss, have to be properly evaluated within the energy audit procedures. In that sense, techniques based on infrared thermography (IRT) have become increasingly popular in recent years due to their quickly obtained and reliable results in envelope inspection and their non-invasive nature [18–21].

2. A Brief Recap of IRT's Key Issues

2.1. IRT in Building Inspection

In the general context of buildings, thermography has been mostly used to investigate aspects of the building envelope [22–24]. In such applications, an IRT sensor can be effectively used to assess the temperature distribution across the interior or exterior closing surfaces, i.e., roofs and walls [25]. Two different approaches to envelope inspection using IRT have been widely implemented: Passive and active. In passive thermography, the surface temperature (ST) is recorded without any external heat stimulation, as the object itself acts as a thermal source. In contrast, active IRT uses an external heat stimulus to increase the thermal contrast (delta-T). For this reason, the second (active) option might be more effective for detecting air infiltrations [26,27]. However, the need for artificial intervention generally poses practical challenges for in-field implementation. Moreover, environmental variables might also interfere with induced thermal flows [28], frequently making active IRT unsuitable for application in real working conditions. Therefore, in this paper, the use of the passive strategy is exclusively analysed.

Passive IRT is typically associated with qualitative analysis, since the main aim is to detect potential anomalies in the thermograms representing defects in the envelope. This approach focused on thermal contrast evaluation is commonly applied in different types of building analysis, e.g., to identify wall areas with an anomalous water content [29–31], to identify points of air leakage and thermal bridges through the building envelope [32–34], or to identify non-visible defects in building structures and materials, such as sub-surface cracks [35]. The procedures for enhancing anomalies in thermograms by means of image processing techniques have also been the subject of several studies (e.g., iterative filtering [36] or principal component analysis [31]).

In contrast, passive IRT is also frequently used for envelope study using a quantitative approach. In this case, the objective is to evaluate the magnitude/importance of the target defect, so the measurement accuracy takes on special relevance [22,37]. In such cases, thermal audit campaigns require an in-depth study of the specific parameters dependent on the material, such as the emissivity and reflected apparent temperature (RAT) [23,38]. Such studies could be feasible under fully controlled laboratory conditions, but in a real operating inspection, the ideal input values for these parameters are almost never achievable [39]. Individual corrections to the emissivity and RAT are difficult to apply in such cases because real scenarios often generate thermograms containing a variety of surface materials. Even directly related parameters involved in the determination of the emissivity and reflectivity (i.e., surface morphology, roughness, oxidation, spectral wavelength, and view angle) may vary considerably within the same thermogram and material. These variations in thermal behaviour pose difficulties in defining an exact emissivity coefficient and justify in part the use of tabulated or reasonably approximate values, assuming an ST reading error that must be quantified.

With changing environmental conditions, such as AAT and relative humidity (RH), not only the thermal conductivity but also the specific heat and density of materials vary, which also may slightly influence the heat transfer through the building envelope. Wind can also significantly influence the heat losses through the building envelope and the thermal measurements over facades and thus should

also be considered [36,40]. Numerical analysis in controlled experiments has allowed useful relations between perceived radiation and climatic parameters, e.g., the modelled atmospheric transmission coefficient [41] or the relation between wind velocity and the Ψ-value (linear thermal transmittance) [42], to be established. Thus, the influence on non-stationary environmental parameters may be, to some extent, reduced by carefully monitoring them during inspection [19].

2.2. Aerial IRT Inspection

The thermography sector has undergone significant advances in the last few decades; for uncooled camera systems, thermal sensitivities (or, equivalently, random noise levels) already reach values <0.03 K in some commercial models. However, the newest revolution in IRT certainly comes from the democratization of unmanned aerial vehicle (UAV) technology and the emergence of lightweight devices easily assembled on board (Table 1). The integration of thermal sensors with drones opens up new possibilities for real-time aerial inspection in many fields. The substantial capture capability of the UAV platforms allows their application in thermal inspection of large areas (e.g., vegetation studies and precision agriculture [43–45], hydrological [46] or industrial inspections, such as those of photovoltaic farms [47,48]).

Table 1. Some commercial thermographic cameras for aerial platforms (updated from Reference [47]).

Manufacturer	Model	Resolution (pixels × pixels)	Thermal Sensitivity (NETD)	Accuracy
FLIR (Wilsonville, US)	Vue PRO 336	336 × 256	0.05 K	Non-radiometric
	Vue PRO 640	640 × 512		
	Vue PRO R 336	336 × 256		±5 °C or ± 5%
	Vue PRO R 640	640 × 512		
FLIR [& DJI (Shenzhen, CN)]	Zenmuse XT 336	336 × 256	0.05 K	Non-radiometric
	Zenmuse XT 640	640 × 512		
	Zenmuse XT2 336	336 × 256		
	Zenmuse XT2 640	640 × 512		
	Duo (+RGB)	160 × 120		Non-radiometric
	Duo R (+RGB)	160 × 120		±5 °C or ± 5%
	Duo PRO R 336 (+RGB)	336 × 256		
	Duo PRO R 640 (+RGB)	640 × 512		
Workswell (Praha, CZ)	WIRIS (2nd Gen) 336	336 × 256	0.03 K	±2 °C or ± 2%
	WIRIS (2nd Gen) 640	640 × 512		
Optris (Berlin, DE)	WIRIS mini	384 × 288	0.05 K	±3 °C or ± 3%
	PI 160	160 × 120	0.04 K	±2 °C or ± 2%
	PI 200/230	160 × 120	0.08 K	
	PI 400	382 × 288		
	PI 450	382 × 288	0.04 K	
	PI 640	640 × 480	0.075 K	
Thermoteknix (Cambridge, UK)	MicroCAM2 384	384 × 288	0.05–0.06 K	Non-radiometric
	MicroCAM2 640	640 × 480	0.06 K	
	MicroCAM3 384	384 × 288	0.05 K	
	MicroCAM3 640	640 × 480	0.04–0.05 K	
Yuneec (Jiangsu, CN)	CGOET	160 × 120	0.05 K	Non-radiometric
	E10T 320	320 × 256		
	E10T 640	640 × 512		
Optix (Panagyurishte, BG)	Minion L	384 × 288	0.05 K	Non-radiometric

The study of building envelopes is perhaps where the fusion of IRT and UAV technologies has the greatest potential [49–52]. UAV-mounted thermal cameras can provide low-altitude aerial images with flexibility and with information about both qualitative and quantitative scenarios. Thus, the method could be particularly well suited to locating difficult-to-access areas of the façade or the roof, where

the thermal conductivity is higher than in areas with thermal bridges, air leakage, or the presence of moisture in the walls.

In summary, assessing thermally related phenomena via passive IRT is possible yet difficult if a quantitative in-field evaluation is intended. The measurements obtained with IRT devices are biased by a number of factors, such as the building material roughness, surface colour or shape [53], thermophysical properties and operating conditions [38], climatic conditions [54], time of day (orientation of the building, sunbeams and shades) [35], the angle of tilt of the sensor and disturbances due to multiple-source reflections [18,22,38]. Both the terrestrial and aerial IRT approaches are susceptible to influence by all these factors. Nevertheless, in the case of a more flexible perspective when positioning the sensor, the angle of tilt in particular should be carefully studied when UAV-mounted thermal cameras are used to achieve reliable accuracies.

The objective of this research is to evaluate the capability and reliability of combining passive thermal IR sensors with low-altitude platforms as building diagnostic tools. More specifically, by presenting the case study of a typical semi-buried wine cellar, four independent steps, directly related with the combination of platform and sensor, were addressed: (i) Assessing the capability of combining lifting platforms and IRT-compatible lightweight sensors in determining building anomalies (qualitative assessment), (ii) finding the optimum lifting platform in terms of operativity and cost, (iii) quantifying the accuracy of thermal imaging systems usually chosen for this type of study (quantitative assessment), and (iv) analysing the impact of the angle of tilt on ST measurements.

3. Materials and Methods

3.1. Study Site

3.1.1. The Building

The study was performed in a cellar situated in O Saviñao (42°33′ N, 7°40′ W, altitude: 399 MAMSL, Figure 1a) within the provincial council of Lugo (Spain). This cellar was built in the late 1920s to produce wines on a small scale. Throughout its history, the structure has undergone several changes and expansions, in accordance with the needs derived from business growth. In most cases, the reforms have not been properly documented (e.g., the internal structures of some of the walls are unknown). These changes have endowed the building with constructive singularities and a diversity of materials. The Southwest façade is half-buried to help maintain a balanced internal AAT throughout the year. Nevertheless, apart from this feature, being an old construction, the cellar does not possess any extra measures for saving energy or maintaining environmental conditions. The outside of the walls is mainly composed of granitic stones, and the roof is covered with red clay tiles. The doors and windows, as well as the framework that supports the roof, are made of wood. Inside, white ceramic tiles are used to cover the walls, and solid ceramic bricks are used for the central pillars and the floor.

Being a semi-buried building is an important characteristic that gives the cellar a high inertia against temperature fluctuations, but practical difficulties have been historically reported for IRT applications in buildings with such a large thermal inertia, as studying their thermal behaviour would require long measurement periods [55]. In this sense, time-lapse experiments using passive IRT methods also encounter several constraints (e.g., the secure and safe positioning of equipment, avoiding occupant interference or unwanted foreground objects, and challenges associated with continuous monitoring of environmental conditions) [56].

In 2005, the owner constructed a new building nearby to house the equipment for the initial wine-processing steps. Since then, the old building (Figure 1b) has been dedicated almost exclusively to ageing the wine in barrels (on the ground floor, Figure 1c) and occasionally to receiving visitors (on the first floor).

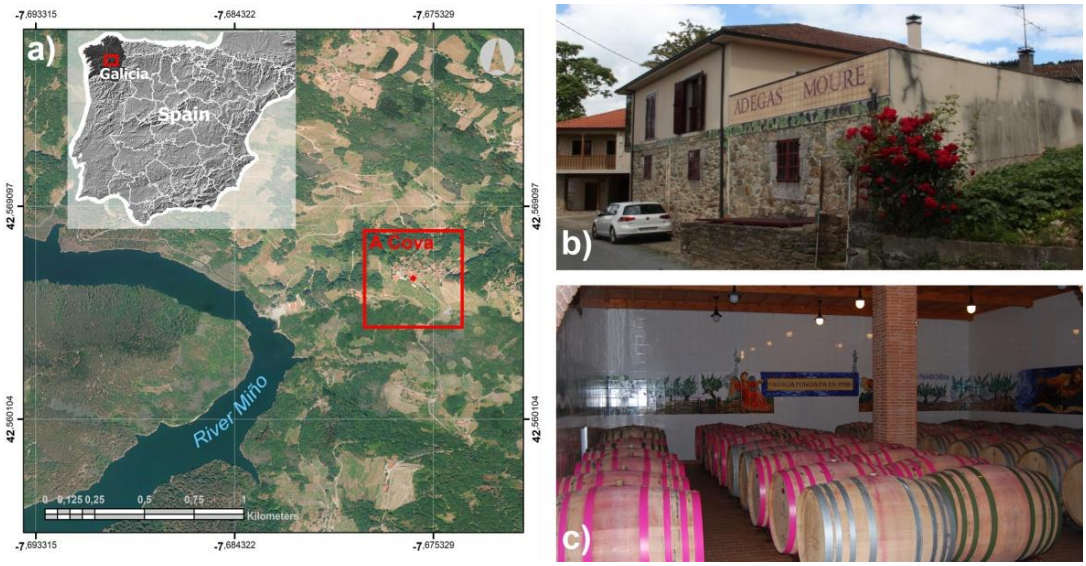

Figure 1. (**a**) Location of the study building (A Cova, Lugo) and images of the cellar from (**b**) outside (main façade) and (**c**) inside the wine-ageing room (ground floor).

3.1.2. The Climate

According to the Spanish Technical Building Code CT-DB-HE [57], several climatic zones can be distinguished in the country. This diversity of zones leads to various wine-producing regions, also known as denominations of origin (or DOs). Specifically, the case study cellar belongs to DO Ribeira Sacra, where the mean annual AAT is approximately 14 °C, and the average annual rainfall is 900 mm. The microclimate of the region shows Mediterranean and continental influences, a consequence of its geographic location as well as its particular orography (steep hillsides along the edges of the Miño and Sil Rivers) [58,59].

3.2. Equipment

3.2.1. Measuring Instruments

The measuring instruments employed were as follows:

–(1×) Hobo data logger (model U12, Onset, Massachusetts, US) (with 4× ext. channels) for measuring the AAT inside the wine cellars. Its parameters included a 0.03 °C resolution and a +0.35 °C accuracy for AAT.

–(2×) Hobo data loggers (model U23-001 Pro v2) for measuring both indoor and outdoor ambient conditions (AAT and RH). Their parameters included a 0.02 °C resolution and a +0.21 °C accuracy for AAT and a 0.03% resolution and a +2.5% accuracy for RH.

–A Temp 7 portable thermometer (XS Instruments, Carpi, IT) equipped with a PT56C contact temperature probe to obtain ST measurements for cross-checking the thermal images. The accuracy of this device was +0.15 °C (120 s).

The locations of the data loggers are represented in Figure 2. The sensors were placed inside the ageing room, on the back side of the central pillar, to protect them from possible abnormal cooling due to air infiltration from open doors or windows. The different channels of the Hobo U12 were situated at height intervals of 90 cm to obtain an average AAT of the room, reducing the effects of convective processes in the measurements. At the same pillar, a Hobo U23 data logger was also placed to register RH and provide a contrast measurement for AAT. The external data were registered by another Hobo U23 data logger, placed on a mast 1 m above the lowest ceiling of the cellar and inside a shield that protected the logger from rain and solar radiation.

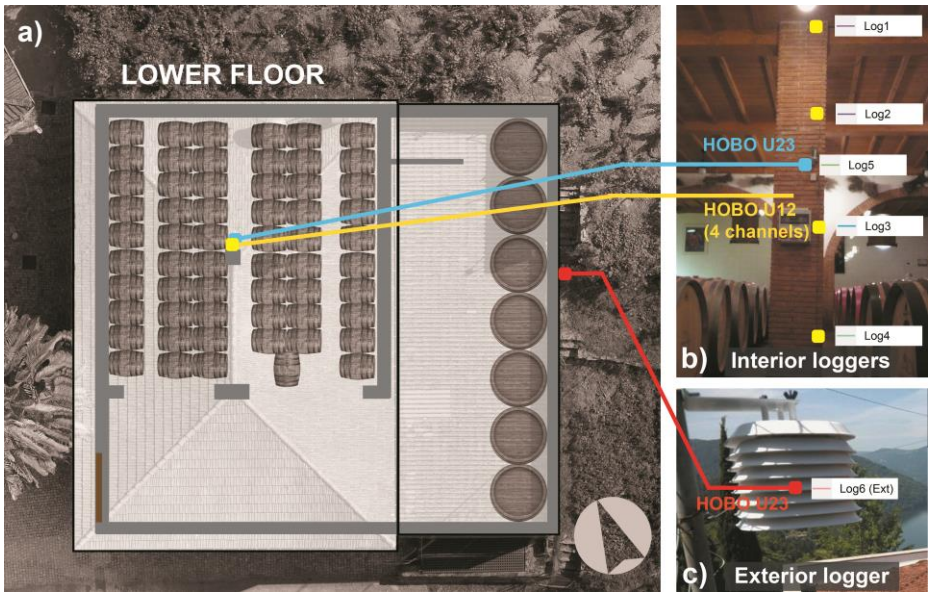

Figure 2. Distribution inside the cellar of the (**a**) logger positions and images of the (**b**) indoor loggers installed in the wall and (**c**) the outdoor logger.

3.2.2. Thermal cameras

Two thermal cameras were chosen to determine the wall ST without contact. The first one was a Vue Pro R (FLIR Systems, Inc., Wilsonville, OR, US), an IR camera specially designed to be mounted onboard a drone. The "R" in the name means "radiometric", which allows this camera to be differentiated from the standard non-radiometric model from the same manufacturer (FLIR Vue Pro). The second IR camera was a FLIR B335, which is a conventional hand-held thermal imaging device. The B335 is also radiometric, which means that both devices allow non-contact measurements of per-pixel calibrated ST. In principle, radiometric devices should more accurately reflect the actual thermal radiance of surface features and thus enable additional post-processing and analysis. The FLIR ResearchIR software package, from the same manufacturer, was employed to perform further analysis of the raw data, allowing tuning of the thermal level and span, colour palette modification, adjustment of parameters such as the emissivity and the reflective temperature and direct importing of environmental time series data from the loggers.

3.2.3. Platforms

To elevate the FLIR Vue Pro R thermal camera to capture images of the exterior of the cellar, a commercial ready-to-fly Drone Quasar UAV (DroneTools, Sevilla, ES) was used. This rotary-wing quadcopter (Figure 3a) has an autonomy of approximately 1 h and a payload of 1.2 kg. A special gimbal provided by the same manufacturer allowed the thermal camera and a conventional RGB mirrorless camera (ILCE α6000, 24 MP; Sony Corp., Minato, JP) with synchronized shoots to be mounted simultaneously. The dual onboard video transmitter allowed the RGB and IRT signal to be transferred from the drone to an audio-visual (AV) screen, giving the pilot a first-person-view (FPV), which guaranteed that the region of interest (ROI) was truly being captured. To compare the operativity of this high range UAV system (~$25,000) with a low-cost alternative lifting method, a simple pole (~$200) was also used. The telescopic device (Figure 3b) used to elevate the FLIR B335 was composed of three main parts. The first part was a (1) telescopic lifting mast (TLM) composed of lightweight materials (aluminium and plastic) with a maximum working length of 7 m. However, working with the pole extended more than 5 m generally requires the help of another operator. At the extreme of the pole, a (2) ball-head mount locked the camera solidly in the desired position. In this case, the adjustable locking system was not included with the pole; therefore, an adapter was attached

to the standard system. Finally, the (3) ground control unit (GCU) also included FPV glasses and the shoot button, which were commercial devices directly wired to the camera. The GCU was designed to be operated by only one person. Table 2 provides a summary of the equipment used.

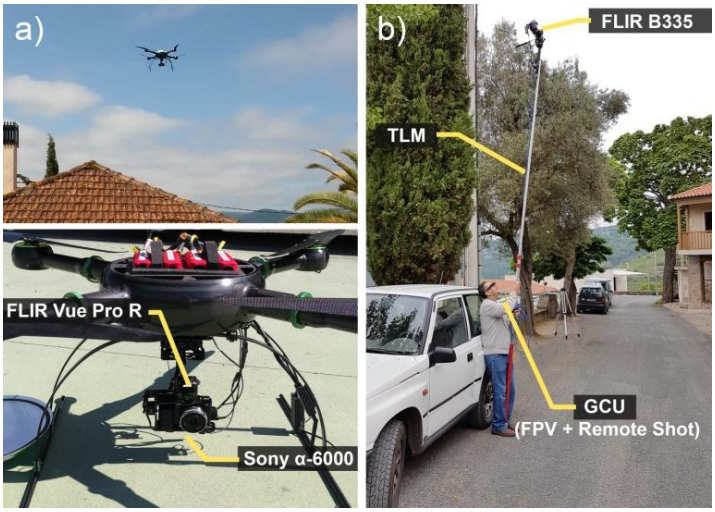

Figure 3. Lifting platforms for the thermal cameras: (**a**) Drone Quasar unmanned aerial vehicle (UAV) and (**b**) telescopic pole.

Table 2. Thermal cameras and platforms used in the study.

Model	Resolution (pixels × pixels)	Thermal Sensitivity (NETD)	Accuracy	Platform	~System Cost (cam. + platform)
FLIR Vue PRO R	640 × 512	0.05 K	±5 °C or 5%	Rotary-wing UAV + 3-axis gimbal	4500 + 25,000 $
FLIR B335	320 × 240	0.05 K	±2 °C or 2%	Extensible pole + fixed ball end	7000 + 200 $

3.3. Data Acquisition and Post-Processing

The measurement campaign took place on the 12 June 2017 and was divided into three independent steps (chronologically, A, B, and C).

The first one (A) involved taking thermograms over common points to perform a comparative assessment in terms of accuracy. Twenty pairs of points apart 30 cm (10 inside and 10 outside the cellar) were selected over uniform surfaces, covering the main surface types of the building (roofs, stone walls, brick walls and painted walls). The points were arbitrarily selected over the surface (avoiding material discontinuities) and marked with sticky tape defining squares 4 cm on a side. To guarantee similar environmental conditions during the capture of images, both the procedures with the pole camera (B335) and those with the drone camera (Vue Pro R) were performed at the same time. Two different operators simultaneously took thermograms from the same distance (3 m) in a direction perpendicular to the surface. The FPV devices systems ensured the images were centred on the points. The contact thermometer was also positioned with an extensible tripod in every scene, registering the ST in the middle of the reference points at the time of the shots and taking the other measurement just after the shots. After post-processing, the mean values of pixels corresponding to the target points were compared with the reference temperatures from the contact thermometer.

In a second step, a similar test (B) was performed with the drone over two fixed points on the SW and SE façades, varying the height (consequently, also the angle of tilt) and keeping a constant distance to the surface of 3 m. Twenty different shots per point were captured, slightly raising the drone between every shot. The heights of the images were automatically determined with the GPS and recorded in the metadata of every image. Thus, the angle could subsequently be easily determined.

The remaining images of the whole envelope were collected in a third step (C), which was simply aimed at qualitatively detecting anomalies. Therefore, these sets of images were taken independently with each system. Notably, the performance of the UAV was much higher than that of the pole-mounted camera, but the operation time of the former was more limited by the battery's duration. For this reason, the procedure with the UAV was completed more quickly. Both the flight and the path for taking images with the pole-mounted camera were planned to cover the entire exterior surface of the building (i.e., the façades and the roof) while minimizing the number of photos. Nevertheless, extra images were taken in areas of particular interest for thermal inspection (e.g., windows, corners, and material discontinuities). Inside the wine-ageing room, due to height limitations, flying the drone was not possible. The entire surface was thermally inspected with the B335 without the pole. In some areas of interest, some photos were also taken manually with the Vue Pro R, after disassembling the camera from the quadcopter.

To prevent the influence of direct solar radiation on the measurements, the outdoor data capture started at 9:00. Then, steps A and C were both repeated indoors, starting at approximately 11:00, just at the end of the outdoor campaign. At this time, the exterior logger registered an AAT 3.5 °C higher than that detected at 9:00, which helped maximize the contrast between the inside and the outside and the detection of potential hot air flows.

The conditions of the wine cellar described above were monitored during the ten days prior to the thermal inspection and on the inspection day. The AAT and RH values inside the cellar were recorded every 5 min during the period from the 2nd to the 12th of June. This month usually marks the beginning of the most problematic period for the ageing of wines because of the rising temperature, which increases the risk of wines being damaged [10]. Particularly, in the month of the test (June 2017), 6 days with a maximum AAT above 35 °C were registered in the area according to the data of the nearby weather station of Pantón (42°32′ N, 7°42′ W, altitude: 340 MAMSL).

Data registered by the loggers were used to correct the atmospheric attenuation, thus improving the reliability of the thermal measurements. The images were post-processed by introducing these environmental parameters (AAT and RH) based on the exact time of every image acquisition. In this case study, the wind effect was considered negligible, as the field campaign was carried out in quasi-steady conditions. The anemometer of the nearby weather station registered speeds <1 km/h during the field campaign, which is considered "calm" according to Beaufort's scale. Due to the wide variability of materials in every image scene, a standard value of 0.95 for emissivity was established [60]. In principle, this value matches the usual tabulated values [61,62] for all the tested materials—red bricks (0.93–0.96), rough granite walls (0.90–0.94), painted walls (0.94–0.96) and red clay tiles (0.88–0.95)—with a reasonable degree of accuracy.

4. Results and Discussion

4.1. Building Diagnosis with IRT

A detailed analysis of the exterior image collection provides a diagnosis of the entire enclosure of the cellar. Several problems, such as the loss of thermal insulation in roof tiles over time (Figure 4a) or the presence of moisture in the walls (Figure 4c), with this method have been detected. Old walls, unlike modern walls, do not have a predictable internal structure and often contain random voids that inhibit moisture flow and hence heat transport [63]. In such cases, qualitative visualization of the imagery usually allows effective interpretation. In this sense, passive IRT is very useful not only for assessing damages or understanding the structure of historical monuments [64–66] but also for characterizing buildings such as this one that have been constructed or refurbished in an unordered manner and whose characteristics are often unknown. Figure 4b shows how a part of the old wall has been maintained in the current enclosure of the cellar, producing a clearly differentiable thermal behaviour (i.e., visible delta-T).

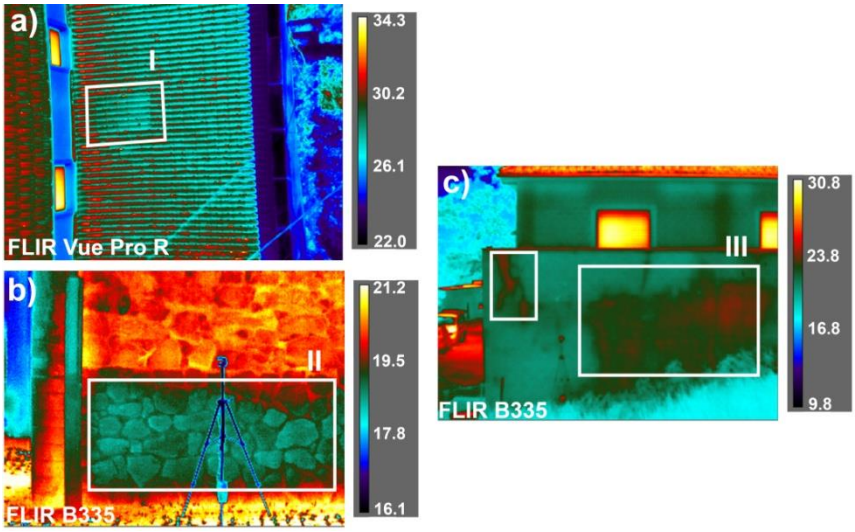

Figure 4. Sample thermal inspection images of the building from the exterior: (**a**) Aerial image of the roof from the drone with the FLIR Vue Pro R and (**b**) and (**c**) two images for wall inspection taken with the FLIR B335. Some detected thermal anomalies are highlighted: (I) a recently replaced group of roof tiles, (II) different coverings of the Southwest façade, and (III) water filtration through wall cracks in the Southeast façade. The temperature scale is in °C.

Detecting interior thermal anomalies was difficult because of the strong influence of the background reflections from the ceramic tiles. Regardless, the inspection of wooden elements of the building (Figure 5) revealed some insulation problems in the joineries and subflooring.

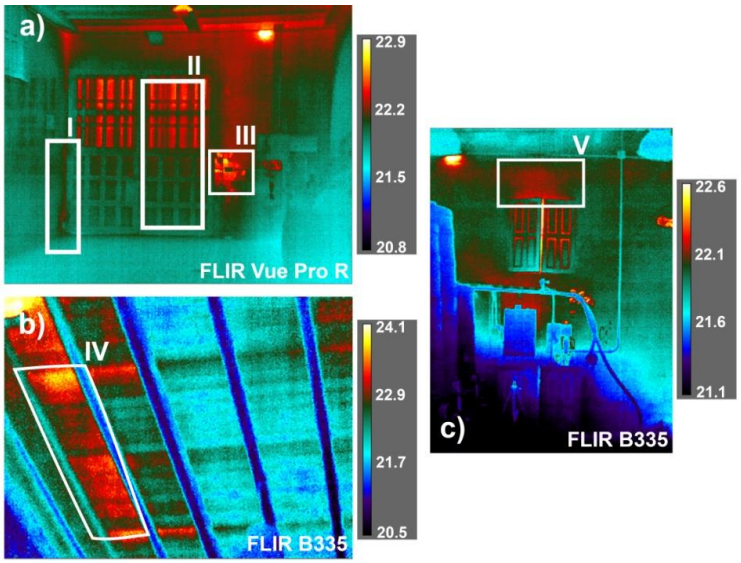

Figure 5. Thermal inspection of joineries inside the cellar: (**a**) Main door, (**b**) wooden ceiling of the wine-ageing room, and (**c**) a wall with a window. Some examples of detected thermal anomalies are highlighted: Air leakages (I) beside the door and (V) above the window, which heat the surface of the surrounding walls, (II) differences in the thicknesses of the upper and lower door leaves, (III) thermal radiation reflected by the ceramic tiles, which introduces noise into the image, and (IV) an area between floor joists with missing insulation. The temperature scale is in °C.

Based on the results, several recommendations that would improve thermal comfort are proposed. The joineries should have mechanisms for thermal bridge breakage, and double glazing should be

applied. Coating the pillars and reinforcing the insulation layer in the subfloor are other recommended measures to improve energy efficiency.

The performances of both tested cameras in the qualitative analysis were overall satisfactory. Even so, it is possible to appreciate some missing details in the thermograms derived from the B335 after testing the cameras from the same distance to the surface (Figure 6). The sensor size is a very relevant parameter for thermal inspection as the number of pixels describing each spatial feature increases with the size of the sensor. The focus and blur of thermograms can also influence the sharpness of the features to be detected.

Figure 6. (**a**) RGB (red-green-blue) images of part of the building and thermograms obtained from the same point (~4 m from the façade) with (**b**) the FLIR Vue Pro R and (**c**) FLIR B335 cameras. The same colour palette and ST scale are used. The temperature scale is in °C.

4.2. The Camera Platform

Obtaining quantitative results for the platform was quite difficult, mainly because the two cameras used with each platform were fundamentally different. However, the thermal survey procedure allowed certain results regarding the suitability of the platforms for the work on this cellar to be obtained.

The first result is about the performance of the two lifting platforms outside the cellar, where both were tested. The capture of some images was planned to be done in a simultaneous manner to obtain comparative thermal measurements, not with the objective of assessing performance. Nevertheless, in this study, the efficiency of the drone far outweighed the performance of the work done with the pole. The total numbers of images taken outside with the drone and with the pole-mounted camera were 321 and 110, respectively, for the same time of acquisition (approx. 1.5 h).

The pole is a quite useful instrument (and much less expensive than the UAV) that allows thermal inspection of buildings without excessive height, such as this building. Even so, the pole used in this case study is a basic model that lacks any system to avoid oscillations at full height. Even with the help of an auxiliary tripod and a second operator, the camera was not easily fully stabilized at heights greater than 5 m. The fixed-head system of the pole is not as flexible as the drone gimbal. This 3-axis motorized gimbal allows the camera to always be oriented at the desired angle to the inspected surface to improve the IR accuracy. The use of a remote pan and tilt system with the pole is almost essential for thermographic inspection. Otherwise, the procedure is much more laborious, since the camera must be lowered to the ground to orient it manually.

Inside the cellar, flying the drone was technically impossible due to the low ceiling. Overall, in closed places or within confined spaces, the pole has demonstrated to be a better alternative because it allows the sensor to approach the ceiling or other elements without risk of collision. In contrast, outdoors, the drone can perform exhaustive capture, including of the most difficult-to-access areas,

such as roofs, without compromising the safety of the operator. The UAV can approach the walls even at full height to obtain a very fine spatial resolution, which allows, for example, visualization of small heat leaks around joineries. The flight can be configured in automatic mode, in which case a single operator can focus on camera handling. However, thermal inspections are usually performed in manual mode with two operators to separately control the aircraft and the camera. The use of the UAV as a lifting platform for the camera is not a trouble-free method. The presence of obstacles in the environment (e.g., power lines, trees, and other buildings), the need to obtain a flight licence and permissions, the dependence on weather conditions, and especially the higher cost of the equipment are some of the important drawbacks.

4.3. Accuracy Assessment of Thermal Images

With the aim of calibrating the readings, the environmental conditions of the cellar (AAT and RH) were monitored during the 10 days prior to the test (Figure 7). Outside the cellar, the maximum AAT registered by the logger was 30.65 °C at 16:15 on the 10 June, the minimum AAT was 7.42 °C at 6:25 on the 5 June, and the average AAT during this period was 17.20 °C. The difference between the maximum and minimum temperatures was quite high (~23 °C), which is typical of a continental climate. Regarding the RH, the maximum value for this period was 99.97%, and the minimum was 30.02%, with a mean of 72.17%.

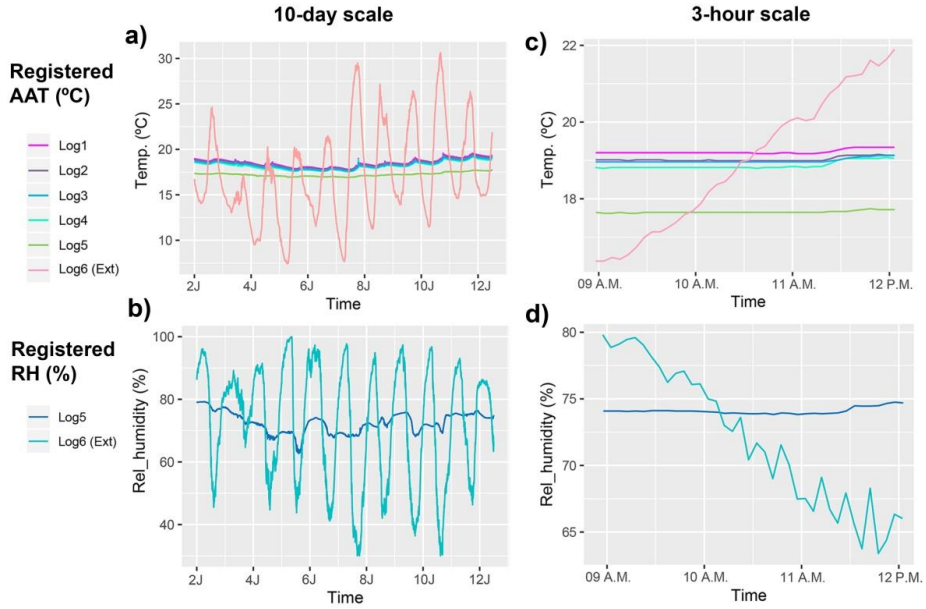

Figure 7. Data recorded by indoor and outdoor data loggers: (**a**) ambient air temperature (AAT) and (**b**) relative humidity (RH) during the 10 days prior to the test (from the 2nd–12 June 2017) and (**c**) AAT and (**d**) RH during the three hours of the thermal imagery campaign (from 09:00–12:00 on 12 June 2017).

Inside the wine-ageing room, the maximum AAT was reached at 18:30 on the 10 June (19.58 °C), and the minimum AAT was reached on the 7 June at 9:05 (16.89 °C). The RH varied from 62.52–79.23%, with a mean value of 72.56% during this period. Because the cellar was a semi-buried structure in contact with the ground, the indoor environment was protected from extreme variations in outdoor conditions.

A total of 20 pairs of points were selected from the entire dataset to perform an accuracy assessment of the measured ST. These images were post-processed with the FLIR ResearchIR software package, taking into account their specific parameters (such as the RH, AAT, and distance to the object). The ST measurements were made twice with the contact thermometer per image (at two points on the inspected surface spaced in height by 30 cm), and the mean value was calculated. Figure 8 shows the comparative results of this test.

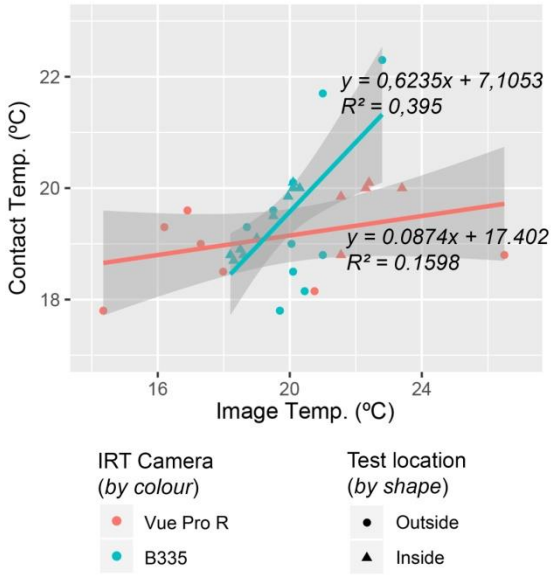

Figure 8. Image-based surface temperature (ST) values vs. contact measurements (PT 56C) for 20 image samples. *The FLIR Vue Pro R camera was disassembled from the quadcopter to take indoor images.

The pole-mounted B335 camera obtained ST values with a bit more correlation (R2 = 0.39) with those taken by the contact probe than did the Vue Pro R camera. The Vue Pro R camera, despite its higher image resolution, which probably makes it better for detecting thermal anomalies, presented less accuracy in the readings. Nevertheless, these results should be interpreted with caution, because being a field test some variables have not been considered, and the results represent the behaviour of the whole system (the pair camera/platform) under real operating conditions. Potential highly influential parameters like emissivity have been used from tabulated values and others like reflections are almost uncontrollable in a field test. Moreover, other internal parameters and camera settings also could have influenced the radiometry captured by the sensor. The Vue Pro R was equipped with the largest focal lenses (f = 19 mm) within its available commercial range of configurations (6.8 mm–19 mm), which might have increased the error in the thermograms. In principle, the larger the field of view (FOV = 2arctan(sensor size/2f)) is, the smaller the error in the temperature measurement is [67]. Therefore, using the same sensor, more accurate measurements are expected with shorter focal lengths.

As expected, the indoor ST data showed less variability than the outdoor ST data in the measurements taken by either of the two thermal cameras (Figure 8). The standard deviation of the ST differential (Tprobe-Timage) outdoors was almost double that indoors (σ = 2.67 and σ = 1.34, respectively). These results are reasonable, as it is easier to obtain stable environmental conditions within the cellar, without exposure to any direct sunlight or wind gusts that could introduce biased readings.

Both radiometric cameras supposedly have the same thermal sensitivity (0.05 °C) but different accuracies (2–5 °C or 2–5% of the reading). Comparatively, the correlations between contact ST measurements and ST from thermograms were quite consistent with the sensor's accuracies provided by the manufacturer. Nonetheless, for some few in-field-sampled points, the errors far outweighed the range of accuracies indicated above, reaching differences >6 °C. Thus, in thermographic ST measuring, it is also extremely important to consider the sources of external uncertainty, especially in real working conditions. The procedure described in Muniz et al. 2014 [68] to obtain combined uncertainty could be useful for estimating errors in those cases. From the law of propagation of uncertainty and considering the input parameters for ST individually, the standard error of thermography can easily exceed 3 °C. Moreover, the analysis of sensitivity revealed a particular influence of emissivity on the uncertainty; therefore, the use of tabulated values is inadvisable for obtaining reliable measurements. It is also important to keep in mind that the contact thermometer has a 0.15 °C resolution with a rectangular

distribution, since it is a digital instrument, but its own measurement uncertainty outdoors can reach values of ~1 °C.

4.4. The Influence of Angle with the Surface

Overall, when a thermal camera is close to a surface, it often records heat not only from the surface itself but also reflected from the background environment. Thus, measuring the ST of very reflective surfaces, such as the ceramic tiles of the cellar, is particularly challenging because of background reflections (e.g., Figure 5a (III)). In these cases, avoiding straight-on measurements is advisable. Too large of an oblique angle can introduce potential biases in radiometric measurement, as it reduces the ability to capture the emissivity of the material and can capture overall reflections from other unwanted sources [69,70]. However, there is evidence that the characteristics of the thermal imager associated with the viewing angle also introduce measurement errors.

Outside the cellar, the coverings of the façades, mainly composed of stones with rough surface textures, did not pose as many reflection problems as the ceramic tiles. Regardless, due to the greater external influence of solar and sky radiation, measurements may also have been affected by reflections. Figure 9a shows the accuracy assessment performed by comparing the radiometric ST values measured with the Vue Pro R camera and the contact probe in relation to the angle of incidence. The contact measurements were taken at fixed points on the SW and SE façades of the cellar, while the images were captured by varying the flight height of the drone.

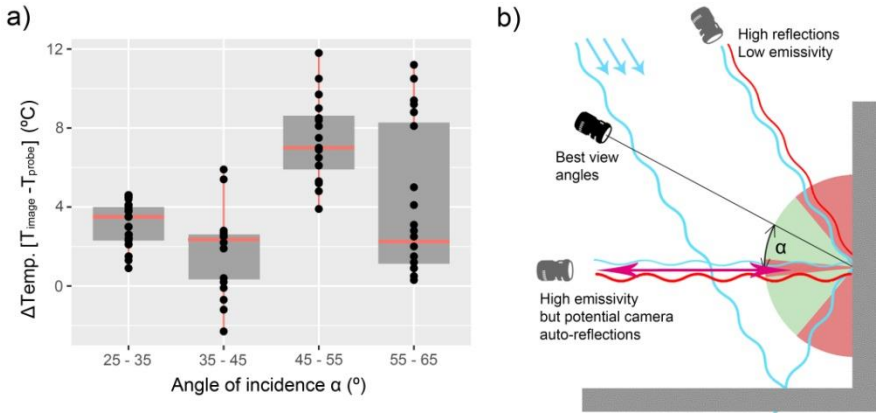

Figure 9. Influence of the angle of incidence on radiometry: The box plot (**a**) shows the differences between image-based ST values and contact measurements (PT 56C) vs. the angle of view, and the sketch (**b**) represents the thermal emission and disturbances due to reflections.

The results show a close relationship between the angle of view and the ST differences recorded (Tprobe-Timage) in the proposed experiment. At angles less than 45°, the majority of the radiation recorded by the sensor is emitted by the surface under inspection. These results are quite consistent with those of other studies [22,67], where the measurement errors were also accentuated by 45–50° maximum tilts. Above these values, the error in the measurement increases drastically due to the influence of reflections from the sky and the sun. Since the reflection phenomena are highly dependent on a number of factors (e.g., time of day, place, atmospheric conditions and surface), the precision of the ST measurement must be analysed for each particular case study. To manage this issue, taking a series of images of the surface over a range of angles is recommended, thereby reducing the influence of any single glint or sky reflection. However, the user should be careful when taking measurements at increasingly oblique angles, as reflections can change and become a more serious issue (Figure 9b). In this regard, it is also important to point out that the UAV gimbal could be manoeuvred to help minimize the effects of the angle of tilt on the perceived emissivity.

5. Conclusions

The application of IRT provides a reliable qualitative assessment method for thermal inspection of a typical wine cellar. Several problems that might compromise the optimal conditions for wine ageing (e.g., moisture in the walls, insulation faults, and heat leakage through the joineries) can be detected through thermal inspection. Thus, the information revealed by thermography facilitates the implementation of corrective measures to ensure optimal environmental conditions for the wine-ageing process. The main proposed reforms are systems for thermal bridge rupture in the joineries and double-glazing windows. Reinforcing the insulation layer in the subfloor and cladding the concrete columns are other recommended measures to improve energy efficiency based on the thermography.

The drone-mounted camera allows for exhaustive image capture, including in the most difficult-to-access areas of the cellar, such as the roofs, without compromising the safety of the operator. However, alternative low-cost lifting methods for low-altitude thermography, such as a simple telescopic pole, can replace the use of a drone when performance is not a priority or when space for manoeuvrability is limited. Even though they are radiometric, the tested B335 and Vue Pro R thermal cameras demonstrate good effectiveness for detecting thermal anomalies, but pose serious difficulties in taking accurate ST measurements. The thermal readings are particularly sensitive to parameters such as emissivity; thus, the use of tabulated or generalized values should be avoided. This fact poses challenges to in-field IRT implementation, as the heterogeneity of scenes can make this technique impractical under a quantitative approach. Noticeably, IRT surveying is always a complex process, but greater difficulties arise in real working conditions due to the difficulty of establishing a completely controlled environment for taking accurate measurements. Among other variables, the angle of view influences the radiometry captured by the sensor and must also be taken into account to avoid disturbances due to specular reflections. Errors in the readings of lightweight devices can easily exceed manufacturer specifications when the tilt angle exceeds 45°.

Author Contributions: Conceptualization, J.O.-S.; methodology, J.O.-S., M.G.-D., M.A.-G. and I.C.-G.; software, M.A.-G., J.O.-S.; formal analysis, J.O.-S., M.G.-D., M.A.-G. and I.C.-G.; writing—review and editing, M.A.-G.; supervision, M.G.-D. and I.C.-G.; funding acquisition, I.C.-G.

Funding: This work was supported by the Spanish Ministry of Science, Innovation and Universities under the National Programme for Research Aimed at the Challenges of Society grant for the project "Bioclimatic Design Strategies in Wine Cellars as Nearly Zero-Energy Building Models" [BIA2014-54291-R].

Acknowledgments: Special thanks are due to Adegas Moure, S.A. for providing access to the cellar.

Conflicts of Interest: The authors declare no conflict of interest.

References

1. Cancela, J.J.; Trigo-Córdoba, E.; Martínez, E.M.; Rey, B.J.; Bouzas-Cid, Y.; Fandiño, M.; Mirás-Avalos, J.M. Effects of climate variability on irrigation scheduling in white varieties of *Vitis vinifera* (L.) of NW Spain. *Agric. Water Manag.* **2016**, *170*, 99–109. [CrossRef]
2. Bonfante, A.; Alfieri, S.M.; Albrizio, R.; Basile, A.; De Mascellis, R.; Gambuti, A.; Giorio, P.; Langella, G.; Manna, P.; Monaco, E.; et al. Evaluation of the effects of future climate change on grape quality through a physically based model application: A case study for the *Aglianico grapevine* in Campania region, Italy. *Agric. Syst.* **2017**, *152*, 100–109. [CrossRef]
3. Crespo, J.; Rigou, P.; Romero, V.; García, M.; Arroyo, T.; Cabellos, J. Effect of seasonal climate fluctuations on the evolution of glycoconjugates during the ripening period of grapevine cv. Muscat à petits grains blancs berries. *J. Sci. Food Agric.* **2018**, *98*, 1803–1812. [CrossRef] [PubMed]
4. Ifie, I.; Abrankó, L.; Villa-Rodriguez, J.A.; Papp, N.; Ho, P.; Williamson, G.; Marshall, L.J. The effect of ageing temperature on the physicochemical properties, phytochemical profile and α-glucosidase inhibition of *Hibiscus sabdariffa* (roselle) wine. *Food Chem.* **2018**, *267*, 263–270. [CrossRef] [PubMed]
5. Styger, G.; Prior, B.; Bauer, F. Wine flavor and aroma. *J. Ind. Microbiol. Biotechnol.* **2011**, *38*, 1145–1159. [CrossRef] [PubMed]

6. Barbaresi, A.; Torreggiani, D.; Benni, S.; Tassinari, P. Indoor air temperature monitoring: A method lending support tomanagement and design tested on a wine-aging room. *Build. Environ.* **2015**, *86*, 203–210. [CrossRef]
7. Zhang, W.; Skouroumounis, G.; Monro, T.; Taylor, D. Distributed wireless monitoring system for ullage and temperature in wine barrels. *Sensors* **2015**, *15*, 19495–19506. [CrossRef] [PubMed]
8. Correia, J.; Mourão, A.; Cavique, M. Energy evaluation at a winery: A case study at a Portuguese producer. In Proceedings of the IManE&E. MATEC Web of Conferences, Iasi, Romania, 24–27 May 2017; Volume 10001, pp. 1–9.
9. Mazarrón, F.R.; Cid-Falceto, J.; Cañas-Guerrero, I. An assessment of using ground thermal inertia as passive thermal technique in the wine industry around the world. *Appl. Therm. Eng.* **2012**, *33–34*, 54–61. [CrossRef]
10. Cañas Guerrero, I.; Martin Ocaña, S. Study of the thermal behaviour of traditional wine cellars: The case of the area of "Tierras Sorianas del Cid" (Spain). *Renew. Energy* **2005**, *30*, 43–55. [CrossRef]
11. Fuentes Pardo, J.M.; Cañas Guerrero, I. Subterranean wine cellars of Central-Spain (Ribera de Duero): An underground built heritage to preserve. *Tunn. Undergr. Sp. Technol.* **2006**, *21*, 475–484. [CrossRef]
12. Mazarrón, F.; Cañas-Guerrero, I. Seasonal analysis of the thermal behaviour of traditional underground wine cellars in Spain. *Renew. Energy* **2009**, *34*, 2484–2492. [CrossRef]
13. Menezes, A.C.; Cripps, A.; Bouchlaghem, D.; Buswell, R. Predicted vs. actual energy performance of non-domestic buildings: Using post-occupancy evaluation data to reduce the performance gap. *Appl. Energy* **2012**, *97*, 355–364. [CrossRef]
14. Guerra-Santin, O.; Tweed, C.; Jenkins, H.; Jiang, S. Monitoring the performance of low energy dwellings: Two UK case studies. *Energy Build.* **2013**, *64*, 32–40. [CrossRef]
15. Demanuele, C.; Tweddell, T.; Davies, M. Bridging the gap between predicted and actual energy performance in schools. In Proceedings of the World Renewable Energy Congress XI, Abu Dhabi, UAE, 25–30 September 2010; pp. 1–6.
16. Bordass, B.; Cohen, R.; Field, J. Energy Performance of Non-Domestic Buildings: Closing the Credibility Gap. In Proceedings of the 8th International Conference on Improving Energy Efficiency in Commercial Buildings, Frankfurt, Germany, 2–3 April 2004; pp. 1–10.
17. De Wilde, P. The gap between predicted and measured energy performance of buildings: A framework for investigation. *Autom. Constr.* **2014**, *41*, 40–49. [CrossRef]
18. Fox, M.; Coley, D.; Goodhew, S.; De Wilde, P. Thermography methodologies for detecting energy related building defects. *Renew. Sustain. Energy Rev.* **2014**, *40*, 296–310. [CrossRef]
19. Nardi, I.; Lucchi, E.; de Rubeis, T.; Ambrosini, D. Quantification of heat energy losses through the building envelope: A state-of-the-art analysis with critical and comprehensive review on infrared thermography. *Build. Environ.* **2018**, *146*, 190–205. [CrossRef]
20. Lucchi, E. Applications of the infrared thermography in the energy audit of buildings: A review. *Renew. Sustain. Energy Rev.* **2018**, *82*, 3077–3090. [CrossRef]
21. Kirimtat, A.; Krejcar, O. A review of infrared thermography for the investigation of building envelopes: Advances and prospects. *Energy Build.* **2018**, *176*, 390–406. [CrossRef]
22. Kylili, A.; Fokaides, P.; Christou, P.; Kalogirou, S. Infrared thermography (IRT) applications for building diagnostics: A review. *Appl. Energy* **2014**, *134*, 531–549. [CrossRef]
23. Cerdeira, F.; Vázquez, M.E.; Collazo, J.; Granada, E. Applicability of infrared thermography to the study of the behaviour of stone panels as building envelopes. *Energy Build.* **2011**, *43*, 1845–1851. [CrossRef]
24. Dufour, M.; Derome, D.; Zmeureanu, R. Analysis of thermograms for the estimation of dimensions of cracks in building envelope. *Infrared Phys. Technol.* **2009**, *52*, 70–78. [CrossRef]
25. Titman, D.J. Applications of thermography in non-destructive testing of structures. *NDT&E Int.* **2001**, *34*, 149–154.
26. Lerma, C.; Barreira, E.; Almeida, R. A discussion concerning active infrared thermography in the evaluation of buildings air infiltration. *Energy Build.* **2018**, *168*, 56–66. [CrossRef]
27. Taylor, T.; Counsell, J.; Gill, S. Energy efficiency is more than skin deep: Improving construction quality control in new-build housing using thermography. *Energy Build.* **2013**, *66*, 222–231. [CrossRef]
28. Bauer, E.; de Freitas, V.P.; Mustelier, N.; Barreira, E.; de Freitas, S.S. Infrared thermography – evaluation of the results reproducibility. *Struct. Surv.* **2015**, *33*, 20–35. [CrossRef]
29. Barreira, E.; Almeida, R.; Delgado, J. Infrared thermography for assessing moisture related phenomena in building components. *Constr. Build. Mater.* **2016**, *110*, 251–269. [CrossRef]

30. Grinzato, E.; Ludwing, N.; Cadelano, G.; Bertucci, M.; Garaganot, M.; Bison, P. Infrared Thermography for Moisture Detection: A Laboratory Study and In-situ Test. *Mater. Eval.* **2011**, *69*, 97–104.
31. Edis, E.; Flores-Colen, I.; de Brito, J. Quasi-quantitative infrared thermographic detection of moisture variation in facades with adhered ceramic cladding using principal component analysis. *Build. Environ.* **2015**, *94*, 97–108. [CrossRef]
32. Kalamees, T. Air tightness and air leakages of new lightweight single-family detached houses in Estonia. *Build. Environ.* **2007**, *42*, 2369–2377. [CrossRef]
33. Barreira, E.; Almeida, R.; Moreira, M. An infrared thermography passive approach to assess the effect of leakage points in buildings. *Energy Build.* **2017**, *140*, 224–235. [CrossRef]
34. Martín Ocaña, S.; Cañas Guerrero, I.; González Requena, I. Thermographic survey of two rural buildings in Spain. *Energy Build.* **2004**, *36*, 515–523. [CrossRef]
35. Bauer, E.; Pavón, E.; Barreira, E.; De Castro, E.K. Analysis of building facade defects using infrared thermography: Laboratory studies. *J. Build. Eng.* **2016**, *6*, 93–104. [CrossRef]
36. Sfarra, S.; Cicone, A.; Yousefi, B.; Ibarra-Castanedo, C.; Perilli, S.; Maldague, X. Improving the detection of thermal bridges in buildings via on-site infrared thermography: The potentialities of innovative mathematical tools. *Energy Build.* **2019**, *182*, 159–171. [CrossRef]
37. Lai, W.W.L.; Lee, K.K.; Poon, C.S. Validation of size estimation of debonds in external wall's composite finishes via passive Infrared thermography and a gradient algorithm. *Constr. Build. Mater.* **2015**, *87*, 113–124. [CrossRef]
38. Tejedor, B.; Casals, M.; Gangolells, M.; Roca, X. Quantitative internal infrared thermography for determining in-situ thermal behaviour of façades. *Energy Build.* **2017**, *151*, 187–197. [CrossRef]
39. Barreira, E.; de Freitas, V.P. Evaluation of building materials using infrared thermography. *Constr. Build. Mater.* **2007**, *21*, 218–224. [CrossRef]
40. Moyano-Campos, J.; Anton-García, D.; Rico-Delgado, F.; Martín-García, D. Threshold Values for Energy Loss in Building Façades Using Infrared Thermography Sustainable. *Sustain. Dev. Renov. Archit. Urban. Eng.* **2017**, *6*, 3859. [CrossRef]
41. Minkina, W.; Klecha, D. Atmospheric transmission coefficient modelling in the infrared for thermovision measurements. *J. Sensors Sens. Syst.* **2016**, *5*, 17–23. [CrossRef]
42. O'Grady, M.; Lechowska, A.; Harte, A. Quantification of heat losses through building envelope thermal bridges influenced by wind velocity using the outdoor infrared thermography technique. *Appl. Energy* **2017**, *208*, 1038–1052. [CrossRef]
43. Sagan, V.; Maimaitijiang, M.; Sidike, P.; Eblimit, K.; Peterson, K.T.; Hartling, S.; Esposito, F.; Khanal, K.; Newcomb, M.; Pauli, D.; et al. UAV-based high resolution thermal imaging for vegetation monitoring, and plant phenotyping using ICI 8640 P, FLIR Vue Pro R 640, and thermoMap cameras. *Remote Sens.* **2019**, *11*, 330. [CrossRef]
44. Khanal, S.; Fulton, J.; Shearer, S. An overview of current and potential applications of thermal remote sensing in precision agriculture. *Comput. Electron. Agric.* **2017**, *139*, 22–32. [CrossRef]
45. Park, S.; Nolan, A.; Fuentes, S.; Hernandez, E.; Chung, H.; O´Connell, M. Estimation of crop water stress in a nectarine orchard using high-resolution imagery from unmanned aerial vehicle (UAV) Digital Vineyards View project Apple Sunburn Risk and Fruit Diameter Estimation Using a Smartphone App View project. In Proceedings of the 21st International Congress on Modelling and Simulation, Gold Coast, Australia, 29 November–4 December 2015.
46. Aicardi, I.; Chiabrando, F.; Lingua, A.M.; Noardo, F.; Piras, M.; Vigna, B. A methodology for acquisition and processing of thermal data acquired by UAVs: A test about subfluvial springs' investigations. *Geomat. Nat. Hazards Risk* **2017**, *8*, 5–17. [CrossRef]
47. Gallardo-Saavedra, S.; Hernández-Callejo, L.; Duque-Perez, O. Technological review of the instrumentation used in aerial thermographic inspection of photovoltaic plants. *Renew. Sustain. Energy Rev.* **2018**, *93*, 566–579. [CrossRef]
48. Zefri, Y.; ElKettani, A.; Sebari, I.; Lamallam, S.A. Thermal Infrared and Visual Inspection of Photovoltaic Installations by UAV Photogrammetry—Application Case: Morocco. *Drones* **2018**, *2*, 41. [CrossRef]
49. Rakha, T.; Liberty, A.; Gorodetsky, A.; Kakillioglu, B.; Velipasalar, S. Heat Mapping Drones: An Autonomous Computer-Vision-Based Procedure for Building Envelope Inspection Using Unmanned Aerial Systems (UAS). *Technol. Des.* **2018**, *2*, 30–44. [CrossRef]

50. Entrop, A.G.; Vasenev, A. Infrared drones in the construction industry: Designing a protocol for building thermography procedures. *Energy Procedia* **2017**, *132*, 63–68. [CrossRef]
51. Kayan, H.; Eslampanah, R.; Yeganli, F.; Askar, M. Heat Leakage Detection and Surveiallance Using Aerial Thermography Drone. In Proceedings of the 26th Signal Processing and Communications Applications Conference (SIU), Çeşme, Turkey, 2–5 May 2018; Volume 1, pp. 1–4.
52. Mavromatidis, L.; Dauvergne, J.; Saleri, R.; Batsale, J. First experiments for the diagnosis and thermophysical sampling using impulse IR thermography from Unmanned Aerial Vehicle (UAV). In Proceedings of the 12th International Conference on Quantitative Infrared Thermography (QIRT 2014), Bordeaux, France, 7–11 July 2014.
53. Cañas-Guerrero, I.; Martín-Ocaña, S.; González-Requena, I. Thermal-physical aspects of materials used for the construction of rural buildings in Soria (Spain). *Constr. Build. Mater.* **2005**, *19*, 197–211. [CrossRef]
54. Lehmann, B.; Ghazi Wakili, K.; Frank, T.; Vera Collado, B.; Tanner, C. Effects of individual climatic parameters on the infrared thermography of buildings. *Appl. Energy* **2013**, *110*, 29–43. [CrossRef]
55. Fang, J.B.; Grot, R.A.; Childs, K.W.; Courville, G.E. Heat Loss from Thermal Bridges. *Batim. Int. Build. Res. Pract.* **1984**, *12*, 346–352. [CrossRef]
56. Fox, M.; Coley, D.; Goodhew, S.; De Wilde, P. Time-lapse thermography for building defect detection. *Energy Build.* **2015**, *92*, 95–106. [CrossRef]
57. Spain Spain CTE-HE. Código Técnico de la Edificación. Basic document HE (Energy saving). June 2017, p. 68. Available online: https://www.codigotecnico.org/images/stories/pdf/ahorroEnergia/DBHE.pdf (accessed on 1 April 2019).
58. Fraga, H.; Malheiro, A.C.; Moutinho-Pereira, J.; Cardoso, R.M.; Soares, P.M.M.; Cancela, J.J.; Pinto, J.G.; Santos, J.A. Integrated analysis of climate, soil, topography and vegetative growth in iberian viticultural regions. *PLoS ONE* **2014**, *9*. [CrossRef] [PubMed]
59. Blanco-Ward, D.; García Queijeiro, J.M.; Jones, G.V. Spatial climate variability and viticulture in the Miño River Valley of Spain. *Vitis J. Grapevine Res.* **2007**, *46*, 63–70.
60. Coutts, A.; Harris, R.; Phan, T.; Livesley, S.; Williams, N.; Tapper, N. Thermal infrared remote sensing of urban heat: Hotspots, vegetation, and an assessment of techniques for use in urban planning. *Remote Sens. Environ.* **2016**, *186*, 637–651. [CrossRef]
61. *CIBSE Guide Volume C—Reference Data*; Chartered Institution of Building Service Engineers: London, UK, 2007.
62. Harvey, L.D. *A handbook on Low-Energy Buildings and District-Energy Systems: Fundamentals, Techniques and Examples*; Routledge: Abingdon, UK, 2012.
63. Brooke, C. Thermal imaging for the archaeological investigation of historic buildings. *Remote Sens.* **2018**, *10*, 1401. [CrossRef]
64. Bisegna, F.; Ambrosini, D.; Paoletti, D.; Sfarra, S.; Gugliermetti, F. A qualitative method for combining thermal imprints to emerging weak points of ancient wall structures by passive infrared thermography—A case study. *J. Cult. Herit.* **2014**, *15*, 199–202. [CrossRef]
65. Kordatos, E.Z.; Exarchos, D.A.; Stavrakos, C.; Moropoulou, A.; Matikas, T.E. Infrared thermographic inspection of murals and characterization of degradation in historic monuments. *Constr. Build. Mater.* **2013**, *48*, 1261–1265. [CrossRef]
66. Lerma, C.; Mas, Á.; Gil, E.; Vercher, J.; Peñalver, M.J. Pathology of Building Materials in Historic Buildings. Relationship between Laboratory Testing and Infrared Thermography. *Mater. Constr.* **2013**, *64*, e009. [CrossRef]
67. Muniz, P.; Cani, S.; Da, S.; Magalhaes, R. Influence of field of view of thermal imagers and angle of view on temperature measurements by infrared thermovision. *IEEE Sens. J.* **2014**, *14*, 729–733. [CrossRef]
68. Muniz, P.; de Araújo Kalid, R.; Cani, S.; da Silva Magalhães, R. Handy method to estimate uncertainty of temperature measurement by infrared thermography. *Opt. Eng.* **2014**, *53*, 074101. [CrossRef]

69. Álvarez-Tey, G.; Jiménez-Castañeda, R.; Carpio, J. Analysis of the configuration and the location of thermographic equipment for the inspection in photovoltaic systems. *Infrared Phys. Technol.* **2017**, *87*, 40–46. [CrossRef]
70. Echániz, T.; Pérez-Sáez, R.B.; Tello, M.J. IR radiometer sensitivity and accuracy improvement by eliminating spurious radiation for emissivity measurements on highly specular samples in the 2–25 μm spectral range. *Meas. J. Int. Meas. Confed.* **2017**, *110*, 22–26. [CrossRef]